Composites based on epoxy resins and poly(3-thiophene methyl acetate) nanoparticles: mechanical and electrical properties

Maria M. Pérez-Madrigal,[1,2,*] Elaine Armelin,[1,2] Denise S. Azambuja,[3] Francesc Estrany,[2,4] and Carlos Alemán[1,2,*]

[1] *Departament d'Enginyeria Química, E.T.S d'Enginyers Industrials de Barcelona, Universitat Politècnica de Catalunya, Av. Diagonal 647, Barcelona E-08028, Spain.*

[2] *Center for Research in Nano-Engineering, Universitat Politècnica de Catalunya, Campus Sud, Edifici C', C/ Pasqual i Vila s/n, Barcelona E-08028, Spain.*

[3] *Instituto de Química, Universidade Federal do Rio Grande do Sul (UFRGS) Av. Bento Gonçalves 9500 - CEP 91501-970, Porto Alegre, RS, Brazil.*

[4] *Departament d'Enginyeria Química, Escola Universitària d'Enginyeria Tècnica Industrial de Barcelona, Universitat Politècnica de Catalunya, Comte d'Urgell 187, 08036 Barcelona, Spain.*

[*]Corresponding authors: m.mar.perez@upc.edu and carlos.aleman@upc.edu

Abstract

Conducting polymer nanocomposites (CPnC) have been prepared by loading different concentrations of poly(3-thiophene methyl acetate) (P3TMA) nanoparticles to an epoxy network. Therefore, the typical limitations of CPs applicability, *i.e.* reduced solubility and difficult processability, have been overcome. The influence of different factors (*i.e.* curing temperature, solvent used to disperse nanoparticles and concentration of P3TMA) on the CPnC properties has been evaluated. The major requirement to obtain homogeneously distributed materials has been found to be the P3TMA-solvent compatibility. Xylene, which is typically used in epoxy resins, has been practically eliminated to avoid the formation of aggregates and has been replaced by tetrahydrofuran. Although properties like chemical structure and doping level, as well as morphology and P3TMA nanoparticle distribution into the epoxy matrix have been examined for CPnC samples, particular attention has been paid to evaluate their mechanical and electrical properties. The Young's modulus and tensile strength values increase upon the addition of a small concentration of P3TMA, independently of the curing temperature, with the exception of 25 wt. % P3TMA composition that exceeds the percolation limit for this material. The electrical dc conductivity determined for samples with 12 and 25 wt. % P3TMA ranged from $6.0 \cdot 10^{-7}$ to $8.2 \cdot 10^{-7}$ S/cm. Therefore, CPnC films exhibited a semiconductor behavior with conductivity values at least three-four orders of magnitude higher compared to that of the pure insulating epoxy (10^{-11}-10^{-13} S/cm).

Keywords: Conducting polymer; Composite; Epoxy resin; Polythiophene; Flexible electronics

Introduction

In recent years, the development of new hybrid materials consisting of the incorporation of conducting particles into an insulating polymer matrix has become a fascinating topic of research [1-3]. This kind of materials presents tailored characteristics combining the fascinating properties of conventional polymers, such as good mechanical performance and thermal stability, with the electrical and electromagnetic features of the conducting element. Moreover, if the conducting element is within the nanometric length-scale (*i.e.* high surface area to volume ratio) and it is correctly dispersed, the interaction between the nanophase and the polymer matrix is enhanced [4]. This leads to a polymer nanocomposite with even better physical and mechanical properties, which is suitable for advanced technological applications: smart textiles [5-6], electromagnetic interference shielding [7-8], stretchable electronics [9-12], electrical actuators [13-15] and bioelectronic devices [16].

A great variety of inorganic conducting fillers, such as metallic powders, carbon black and carbon nanotubes, have been employed for monitoring the electromagnetic properties of stretchable composite films [17-19]. Lately, these inorganic conducting fillers have been gradually replaced by intrinsically conducting polymers (CPs) because of their lower density, mild polymerization conditions and good electrical properties. Nevertheless, the applicability of CPs is limited by their reduced solubility in common organic solvents, difficult processability and poor mechanical properties. Despite these drawbacks, polyaniline (PAni) has been successfully incorporated into polyurethane [20] and epoxy resin matrices [21-23]. On the other hand, polythiophene (PTh) derivatives incorporating suitable substituents into the 3-position of the thiophene ring represent an attractive alternative among CPs, since they show good solubility, excellent environmental stability, good electrical properties and the possibility of

functionalization. Therefore, several studies have been focused on the preparation of stretchable composites by including PTh derivatives as the conducting filler [24-26].

Epoxy resins are thermosetting polymers that exhibit high tensile strength as well as chemical and corrosion resistance. For these reasons, epoxy resins are extensively used in a wide range of industrial applications, such as surface coatings, adhesives, painting materials and in electronic devices. More specifically, epoxy resins based on diglycidyl ether of bisphenol A with epichlorohydrin are among the most commonly used, and are normally cured with polyamines, as hardener. In a very recent study, Zabini *et al.* [27] obtained a new conducting epoxy nanocomposite that included PTh nanoparticles. In addition to the expected increment in the electrical conductivity, PTh nanoparticles provoked a significant improvement in both the mechanical performance and thermal stability.

Inspired by the importance gained by CPs in hybrid materials, the present study aims to obtain and characterize a new CP nanocomposite (CPnC) by incorporating nanoparticles of poly(3-thiophene methyl acetate) (P3TMA) to an epoxy resin. This PTh derivative bears a carboxylate group, which is attached to the 3-position of the thiophene ring, and shows easy solubility in different solvents and good solution processability. Previous studies used P3TMA as conducting filler in a poly(vinylidine fluoride) (PVDF) matrix. More specifically, Manna *et al.* [28] blended nanostructured P3TMA with PVDF by means of a reactive blending technique. More recently, Gomes *et al.* [29] prepared and characterized a blend made of P3TMA and PVDF using a synthetic approach based on a photochemical reaction. Despite of these antecedents, no previous study has been reported of a CPnC based on P3TMA and epoxy resins.

Firstly, homogeneous CPnC films were prepare by the most efficient approach, which considered different aspects related to the resin, the mixing process, the curing

temperature and the solvent. The resulting composites were evaluated by FTIR and UV-vis spectroscopy techniques to analyze their chemical structure and the doping state of P3TMA, respectively. Then, as both the mechanical and electrical properties of CPnC films are considered of major importance, special attention has been paid to study the influence of the P3TMA loading content on the stress-strain response of the prepared materials, while the CPnC electrical features, which represent an essential property of this new hybrid material, have been extensively examined by the two-point probe test and electrochemical impedance spectroscopy (EIS). Finally, morphological and topographical observations have been carried out by scanning electron microscopy (SEM) and atomic force microscopy (AFM) to monitor the dispersion of P3TMA nanoparticles on the epoxy matrix, and determine its influence on the mechanical and electrical properties of CPnC films.

Methods

Materials. Commercial epoxy resins based on bisphenol A and epichlorohydrin were used in this study. More specifically, the resin solution, hereafter denoted Liquid Epoxy (LEP), is commercialized under the trade name of EPIKOTE™ 1001X75 and consists of diglycidyl ether of poly(bisphenol A-*co*-epichlorohydrin) in xylene (75 wt.% of resin). The solid resin used in this work, which is commercialized under the trade name EPIKOTE™ Resin 1001, has the same composition than EPIKOTE™ 1001X75 but is completely free of solvent. It is hereafter denoted Solid Epoxy (SEP). Both products are produced by Hexion Specialty Chemicals (USA) and were gently provided by Brenntag Quimica, S.A.U (Spain). Resin epoxy equivalent, epoxy group content and molecular weight were 450-500 g/eq, 2000-2220 mmol/kg and 880 g/mol, respectively.

CRAYAMID 195X60, hereafter denoted Polyamide Hardener (PAH), was used as the curing agent for both resins. This resin, which is produced at 60 wt.% solid content in xylene by Helm Products (USA), was kindly provided by Arkema Coating Resins S.A.U. (Spain). The hardener typical active hydrogen equivalent weight, total amine value and viscosity assessed at 25 ºC were 240 g/eq, 240-270 mg KOH/g and 3000-6000 mPa·s, respectively, as specified by the producer. Considering that each epoxy group reacts with one reactive hydrogen, the resulting epoxy:polyamide mix ratio was approximately 65:35 based on the solid resin composition. All products were used as received. Scheme 1a shows the chemical structure of bisphenol A based resins.

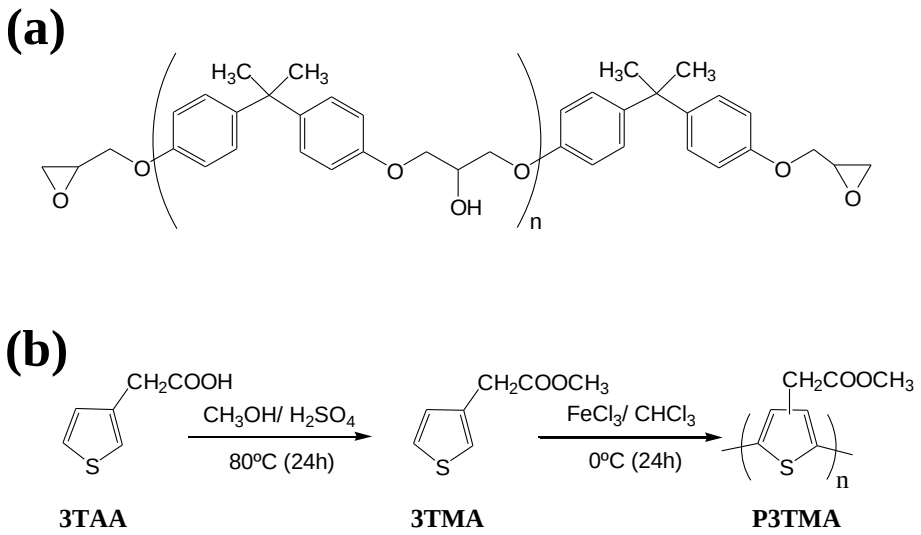

Scheme 1. (a) Chemical structure of bisphenol A based resins. (b) P3TMA synthesis steps.

3-Thiophene acetic acid (3TAA) (98.0%) was purchased from Fluka (Poland). Iron chloride anhydrous (97.0%), dry methanol (99.5%), chloroform (99.9%) and tetrahydrofuran (THF) stabilized with 300 ppm of BHT-PRS (99.5%) were purchased from Panreac Quimica S.A.U. (Spain) and used as received, without further purification.

P3TMA synthesis. P3TMA (Scheme 1b) was prepared using a two-step process. In the first one, 3-thiophene methyl acetate (3TMA) was obtained by refluxing 3TAA, which was the starting monomer, in dry methanol for 24 hours and at 80 ºC. After this, P3TMA was obtained by chemical oxidative coupling polymerization in dry chloroform using anhydrous ferric chloride ($FeCl_3$) as oxidant and dopant, following the procedure described by Kim and co-workers [30]. Purified 3TMA monomer was obtained with 74% of yield, while the yield of P3TMA, which was a red-brown powder, was 61% after removing the residual oxidant and oligomers.

***Preparation of epoxy:P3TMA CPnC films*.** A 0.5 wt. % stock P3TMA solution was prepared by dissolving a given amount of P3TMA powder in THF, which was compatible with the three components of the system (*i.e.* the epoxy resin, the hardener and the CP). A pre-treatment, which consisted of 10 minutes sonication, was applied to P3TMA before (*i.e.* as a powder) and after its dissolution in THF. Finally, the solution was cotton-filtered and magnetically stirred for two hours to stabilize.

In a first stage, LEP/P3TMA films were prepared by considering two different mixing routes. In the first one (route R), the P3TMA solution was mixed with the LEP resin in the proportions appropriated for desired composition. After 5 hours stirring, the adequate curing agent amount was added. In the second route (route H), the P3TMA solution was initially mixed with the PAH resin and, after 5 hours of stirring, the LEP resin was added. Once the resin epoxy and the hardener were in contact, mixtures were treated in the same way, independently of the applied route: 4 minutes of manual mixing with a glass rod, 15 minutes of settling, 4 minutes of manual mixing, and finally 15 minutes of waiting. As a general notation, the content of the P3TMA filler in the CPnC, which was 1, 3, and 5 wt. %, is expressed as the ratio of P3TMA mass to the total mass of the nanocomposite after complete solvent evaporation. Therefore, samples

were codified as, for example LEP/P3TMA-R1, according to the use of liquid epoxy resin, route R and 1% of P3TMA additive.

In a second stage, the solid epoxy resin was used and, therefore, the P3TMA solution was incorporated to the SEP resin (without xylene). For this composite film preparation only the route R was applied and samples were called SEP/P3TMA-RX (X being the content of P3TMA), as explained above. For this purpose, the SEP resin was dissolved in THF at a 60 wt. % concentration before mixing with the P3TMA nanoparticles. Furthermore, the xylene solvent of the commercial hardener was evaporated slowly under controlled conditions (light protection) until less than 10 wt. % of its original content remained. Then, the hardener was dissolved again in THF to a 60 wt. % concentration. This approach allowed us to increase the P3TMA content in the CPnC films to 12 and 25 wt. % due to the good dispersion of the CP in THF solvent.

CPnCs were manually deposited onto glass dishes which were previously coated with Teflon®. Both systems, LEP/P3TMA and SEP/P3TMA, were cured at room temperature (RT) or 60ºC (T60) during the first 24 hours. Then, all films undertook a second curing step at room temperature during 3 days. The thickness of the resulting films ranged from 50 to 180 μm while their color varied from dark yellow to brown red depending on the P3TMA concentration.

FTIR and UV-vis spectroscopies. In order to determine the size of P3TMA nanoparticles in the solution, static light scattering (SLS) measures were performed with a Vasco Particle Size Analyzer (Corduan Technology). The software NanoQ was used for data collection and evaluation.

FTIR absorption spectra were recorded on a FTIR Jasco 4100 spectrometer. Samples were placed in an attenuated total reflection accessory (top-plate) with a diamond crystal (Specac model MKII Golden Gate Heated Single Reflection Diamond ATR).

For each sample 32 scans were performed between 4000 and 600 cm^{-1} with a resolution of 4 cm^{-1}.

UV-vis absorption spectra of the CPnC films were obtained using a UV-vis-NIR Shimadzu 3600 spectrophotometer equipped with a tungsten halogen visible source, a deuterium arc UV source, a photomultiplier tube UV-vis detector, and a InGaAs photodiode and cooled PbS photocell NIR detectors. Spectra were recorded in the absorbance mode between 300 and 800 nm using the integrating sphere accessory (model ISR-3100). The interior of the integrating sphere was coated with highly diffuse BaO reflectance standard. Single-scan spectra were recorded at a scan speed of 60 nm/min. Measurements, data collection and data evaluation were controlled by the computer software UVProbe version 2.31.

The optical π-π^* lowest transition energy (E_g) or band gap energy was determined considering the following expression:

$$E_g(\text{eV}) = \frac{h \cdot c}{1.6 \cdot 10^{-19} \cdot \lambda_{onset}} \qquad (1)$$

where h (Plank's constant) = $6.626 \cdot 10^{-34}$ J·s, c (speed of light) = $3.0 \cdot 10^{8}$ m/s and λ_{onset} (m) is the cut off wavelength for the absorption spectra.

Mechanical properties. A Zwick Z2.5/TM1S (Zwick GmbH & Co KG, Germany) machine was used to perform uniaxial elongation tests for rectangular samples (n =10) with an area of about 30 × 3 mm^2 and a variable thickness. Tensile testing was conducted at room temperature and samples were strained at a constant deformation speed of 10 mm/min. The Young's modulus was determined from the slope in the linear elastic region (*i.e.* below 5 % strain).

Electrical characterization: dc conductivity and EIS measurements. The electrical dc conductivity was determined using the two-point probe procedure and an electrometer, varying the temperature from 35 to 130ºC at intervals of 25ºC.

For electrochemical impedance spectroscopy (EIS) measurements, appropriated sized CPnC films were cut to get an area of 1.767 cm^2 and sandwiched between two stainless steel (AISI 316L) electrodes (diameter = 1.5 cm) assembled into an isolating holder. The cell was tightened with screws. However, prior cell closing, samples were immersed in buffered saline solution (PBS, pH = 7.4) at room temperature for 24 hours, water excess being wiped out with a tissue. EIS measurements were performed using an AUTOLAB PGSTAT302N in the 100 kHz - 10 mHz frequency range and sinusoidal voltage amplitude 10 mV. All experiments were carried out at room temperature. After data collection, EIS results were then processed and evaluated using the Frequency Response Analyser software (FRA software, Eco Chemie B.V, version 4.9.007).

Morphological characterization: SEM and AFM. The cross-sections of CPnC films were examined by scanning electron microscopy (SEM) using a Focused Ion Beam Zeiss Neon40 scanning electron microscope equipped with an energy dispersive X-ray (EDX) spectroscopy system and operating at 5 kV. Samples were freeze-fractured with liquid nitrogen and mounted vertically onto specific supports using adhesive silver paint. Then, samples were sputter-coated with a thin carbon layer of 6-10 nm using a K950X Turbo Evaporator to prevent electron charging problems.

Atomic force microscopy (AFM) studies were conducted to obtain topographic data for CPnC films surface with an AFM Multimode™ (Veeco) and a NanoScope controller under ambient conditions in tapping mode. Images were taken using a silicon TAP 150-G probe (Budget Sensors, Bulgaria) with a frequency of 150 kHz and a force constant of 5 N/m was used. The Root Mean Square roughness (RMS Rq), which is the average height deviation taken from the mean data plane, was determined using the statistical application of the Nanoscope software.

Results and Discussion

Preparation of epoxy:P3TMA CPnC films

P3TMA particles have to be distributed throughout the sample creating effective electron conductive paths to obtain an electrically active P3TMA network within the epoxy matrix. Therefore, as a first measure to prevent particle aggregation, P3TMA nanoparticles were mildly sonicated before and after its dissolution in THF. SLS measures allowed us to determine the dimensions of P3TMA particles in the stock solution (0.5 wt. % P3TMA) before their addition to the epoxy resin (route R) or to the curing agent (route H). Results indicate that the diameter of almost 90 % of P3TMA particles in the solution is below 170 nm. The size of the remaining 10 % varies from 1.1 μm to 2.6 μm. However, even though solute-solute electrostatic interactions provoke the aggregation of P3TMA nanometric particles to a small extent, solute–solvent interactions prevail, leading to a homogeneous dispersion of P3TMA particles. More specifically, the heterocycle of THF molecules, which resembles the thiophene ring in the P3TMA structure, is the most influent factor for the good solubility of P3TMA in this organic solvent.

LEP/P3TMA system produced films with significant phase separation due to the incompatibility of P3TMA with the high concentration of xylene present in both EPIKOTE™ 1001X75 and CRAYAMIDE 195X60. Films exhibited air bubbles and P3TMA particles were highly concentrated around the edges. In those films, P3TMA particles were agglomerated regardless P3TMA concentration, curing temperature or mixing route. Thus, to attenuate the incompatibility between P3TMA and the solvent during the nanocomposite film processing, the preparation of SEP/P3TMA system was focused on substituting the xylene solvent by THF almost completely. As a result, CPnC films produced using the solid epoxy resin, applying route R (SEP/P3TMA-RX)

and CRAYAMID 195X60 as the hardener element were more homogeneous and defect-free. Optical micrographs showed no significant differences between samples considering P3TMA composition, apart from the increasing red color intensity with P3TMA content. On the other hand, films obtained from route H (SEP/P3TMA-HX) were discarded due to rapid particle aggregation. Finally, although the solvent plays an important role in P3TMA aggregation, high-quality SEP/P3TMA-RX films were successfully prepared by a straightforward procedure, and their properties were further characterized.

FTIR and Uv-vis spectroscopy

Before evaluating the mechanical and electrical properties of SEP/P3TMA-RX films, FTIR spectroscopy was used to characterize their chemical structure, as well as to assess the completion of the epoxy curing process. Figure 1 presents the FTIR spectra for P3TMA and SEP/P3TMA-R0, SEP/P3TMA-R1 and SEP/P3TMA-R25 samples cured at 60 ºC in the range from 1800 to 700 cm^{-1}. Results evidence the formation of physical blends by the overlapping of absorption bands coming from the epoxy matrix and P3TMA. Specifically, the ester C=O stretching absorption is detected at 1731 cm^{-1} (peak A in Figure 1), while the C=C thiophene ring stretching appears at 1520 cm^{-1} (peak B). Moreover, asymmetric CH_3 bending (peak C) and both symmetric and asymmetric CH_2 bending (peak C') from P3TMA contribution are located at 1432 and 1408 cm^{-1}, respectively. As it was expected, the intensity of these bands increases with P3TMA concentration, and results corroborate that CPnC films exist only as a physical mixture of its components.

To evaluate the completion of the epoxy curing process one of the most important absorption bands is that of the oxirane ring, which appears at *ca.* 915 cm^{-1}. The intensity

of this peak decreases as the curing process occurs. Moreover, new absorption bands appear at 1645 and 1550 cm^{-1} due to the stretching and bending of the amide moiety coming from the hardener. Exactly the same peaks were observed by samples cured at room temperature. Thus, all CPnC samples underwent a complete crosslinking process regardless the curing procedure (RT or T60) or P3TMA wt. % content since no peak is detected at *ca.* 915 cm^{-1}. At this point, all reported data refer to samples cured at 60 °C to avoid duplicative results with samples cured at RT.

On the other hand, UV-vis absorption spectra were recorded in the range from 300 to 800 nm to evaluate the doping level and electronic state of the conducting filler in CPnC films. Figures 2 displays the spectra for films cured at 60 ºC, while the values for λ_{max}, λ_{onset} and E_g obtained for each CPnC film are listed in Table 1. Furthermore, UV-vis spectra recorded for the epoxy film without P3TMA as well as for a diluted P3TMA solution in THF (0.001 wt. % P3TMA) are also shown as control samples.

The absorbance peak displayed at λ_{max} = 400 nm for SEP/P3TMA-R1 corresponds to the lowest π-π^* transition of the thiophene ring in P3TMA [31-32], which does not appear in the pure epoxy sample. When increasing the P3TMA concentration, the π-π^* transition band exhibits a red shift, independently of the curing temperature. For example, λ_{max} shifts from 400 nm for SEP/P3TMA-R1 to 538 nm for SEP/P3TMA-R25. This indicates that the energy required for the π-π^* transition decreases since the π-conjugation length increases, enhancing the absorption intensity. Intermolecular interactions between the conductive filler and the epoxy matrix may explain the red shift. However, this behavior may be also attributed to the aggregation of P3TMA particles in CPnC films with higher P3TMA concentration, which causes delocalization of the π-electrons because of the π-π stacking interactions. This red shift was also observed by Manna *et al.* [28] in nanocomposites made of P3TMA (filler) and

poly(vinylidene fluoride) (matrix). These authors suggested that the root-mean-square end-to-end distance of P3TMA chains decreases with increasing aggregation, thus leading to a delocalization of the π-orbitals.

As the curing is a thermally activated process, temperature stimulated the epoxy sites reactivity increasing the cross-linking reaction rate and leading to a much faster and more complete curing degree. Therefore, a dense epoxy network is expected to be obtained at 60ºC, P3TMA particles being entrapped quicker in the formed epoxy matrix than in that produced at RT (Figure 3). Furthermore, fast cross-linking induces phase separation at microscopic scale (*i.e.* small aggregates) while slow curing (*i.e.* lower network density) results in larger aggregates [23]. Considering this discussion, which was confirmed during morphological characterization by SEM and AFM (see section below), the slightly lower red shift observed for CPnC films cured at 60ºC (Table 1) has been understood in terms of P3TMA aggregation size and intrachain interactions. This reasoning is clearly observed for SEP/P3TMA-R12 films. When curing at RT, the high content of P3TMA leads to a major aggregation of particles and SEP/P3TMA-R12 (RT) and SEP/P3TMA-R25 (RT) films behave similarly in terms of E_g (1.97 eV and 1.94 eV, respectively). However, when the system is cured at 60 ºC, P3TMA nanoparticles do not aggregate, SEP/P3TMA-R12 (T60) bandgap energy behaving more as SEP/P3TMA-R5 (T60) (2.13 eV and 2.25 eV, respectively). Therefore, results evidence that in addition to the solvent influence the curing temperature is another important factor in P3TMA aggregation.

Mechanical properties

It is well known that the incorporation of nanoparticles into a polymer matrix results in the modification of its mechanical properties [13]. In general, the stiffness of the

polymer matrix increases with the increasing filler content. Bearing that in mind, SEP/P3TMA-RX films were characterized by means of the standard uniaxial tensile test to evaluate the effect of different P3TMA wt.% content on their mechanical properties, and thus establish the optimum filler concentration. Figure 4a shows representative strain-stress curves for CPnC films cured at 60 ºC, and the resulting mechanical properties are summarized in Table 2**.** As it can be seen, the stress-strain curves for CPnC films show a linear behavior until the breaking point.

The Young's modulus increases from 825 MPa ± 142 MPa (SEP/P3TMA-R0) to 1010 MPa ± 204 MPa (SEP/P3TMA-R1) after adding only 1 wt. % P3TMA. Following this trend, the Young's modulus of CPnC films cured at T60 increase with P3TMA concentration until 5 wt. % P3TMA, where the maximum is reached (1192 MPa ± 164 MPa). However, when 25 wt.% P3TMA is added, the Young's modulus deteriorate (SEP/P3TMA-R25) compared to that of the epoxy film without CP, independently of the curing temperature (Figure 4b), which represents a collapse of the CPnC. The film is excessively brittle and does not undergo deformation at all, as its strain at break value is only 1.1% (Figure 4a). The excessive number of restriction points created by the high agglomeration of P3TMA particles prevents the epoxy polymer chains to absorb the strain, and thus resulting in films with no practical application. Moreover, for CPnC films cured at RT, P3TMA particle aggregation plays a crucial role. Concretely, the highest Young's modulus values are reached at 1 and 3 wt.% P3TMA (Figure 4b, RT). However, when P3TMA content increases, instead of more CP particles better dispersed, larger P3TMA aggregates are formed, which cause a lesser reinforcement effect, and thus lower Young's modulus values are obtained. In contrast, films cured at T60 behave similarly to nanocomposites with increasing nanoparticle content, as

P3TMA particles act as motion restricted points leading to a stiffer and more fragile material.

Besides, all CPnC films exhibit improved tensile strength with respect to epoxy films without CP for all compositions, except for that with 25 wt. % P3TMA (Table 2 and Figure 4a). Moreover, the tensile strength shows a maximum value at 5 wt. % P3TMA content (63 MPa ± 4 MPa). Otherwise, the introduction of P3TMA particles leads to films with similar elongation at break values compared to that shown by pure epoxy. Therefore, results indicate that the optimum P3TMA wt. % content regarding mechanical properties is reached at around 5 wt. % P3TMA for films cured at 60 ºC.

In general terms, the presence of P3TMA particles, which restricts the motion and deformation of epoxy macromolecular chains, and the strong interaction (*i.e.* good compatibility and attractive cohesive forces) between the epoxy network and the conducting filler provoke the stiffening of the material (increased Young's modulus and tensile strength values). However, SEP/P3TMA-RX films containing up to 12 wt. % P3TMA display enhanced strain at break response compared to that of pure epoxy films. Hence, CPnC films exhibit a good mechanical performance despite the addition of conductive nanoparticles, which enables the system to be used in advanced industrial applications with those specific mechanical requirements.

Electrical characterization: dc conductivity and EIS measurements

In the design of conducting hybrid materials, not only an adequate mechanical response is important, but the system has to display enhanced electrical properties. In this particular case, P3TMA was chosen as conductive filler because of its good electrical properties and solubility in THF, the only organic solvent compatible with all the elements of the system, which minimizes particle aggregation.

The electrical dc conductivity of CPnC films with different P3TMA content and cured at RT and T60 was firstly assessed by the two-point probe method. Tests were carried out from 30ºC to 130ºC at intervals of 25ºC. Pure epoxy samples are electrically insulating, and thus their conductivity is extremely low. SEP/P3TMA-R0 (RT and T60) samples exhibit conductivity values lower than 10^{-8} S/cm, which is the equipment lower resistance limit. As reference, for Leyva *et al.* [22] the conductivity of a similar epoxy network based on diglycil ether of bisphenol A was determined to be ~ $4 \cdot 10^{-11}$ S/cm, whereas for Zabihi *et al.* [27] it was in the order of 10^{-14} S/cm. Thus, it can be assumed that pure epoxy films displayed an electrical dc conductivity value in an intermediate order of magnitude, which is considered virtually null (10^{-13} S/cm).

Similarly, CPnC samples with 1, 3 and 5 wt.% P3TMA exhibit very low conductivity values (below ~10^{-8} S/cm) since no register was possible regardless the increment in the testing temperature. On the other hand, samples with the highest P3TMA content, 12 and 25 wt. % P3TMA, show an increase in the electrical dc conductivity value at high temperatures. Concretely, the electrical conductivity for SEP/P3TMA-R12 and SEP/P3TMA-R25 samples was determined to be between $6.0 \cdot 10^{-7}$ S/cm - $7.2 \cdot 10^{-7}$ S/cm and $6.5 \cdot 10^{-7}$ S/cm - $8.2 \cdot 10^{-7}$ S/cm, respectively. Films exhibit a semiconductor behavior with conductivity values at least four orders of magnitude higher compared to that of the pure epoxy. To improve the electrical properties of P3TMA and achieve higher conductivity values, CPnC samples were immersed in two doping solutions containing HCl (0.1 M) or $FeCl_3$ (5 wt%) for 6 hours. However, no significant increase in the conductivity was observed.

For all samples, the reduced conductivity values obtained at low testing temperatures confirm that the red shift observed in UV-vis spectra results is not due to an increase in the conjugation length of P3TMA, but to the aggregation of its chains by the π stacking

process. Although having achieved a high degree of dispersion, P3TMA particles are not enough interconnected in the epoxy matrix and the electron conduction path is interrupted, this behavior being practically independent of the P3TMA content and the curing temperature when testing at low temperatures. However, there is an increase in the conductivity value with the P3TMA content when the testing temperature reaches 120 ºC since P3TMA chains move and the high content of P3TMA particles facilitates the interaction among them. This change in the polymer chains conformation results in the creation of a small number of conductive regions which are able to develop conduction paths, revealing the semiconducting nature of CPnC films.

It should be mentioned that PTh derivatives present low electrical dc conductivity values (~10^{-3} S/cm) [33-35] as compared to other CPs, which should be attributed to the presence of side groups close to the π-conjugated backbone. Thus, particularly in P3TMA, the carboxylate group is known to affect the electron transport through the π-system [35]. Previous studies obtained similar results when mixing P3TMA with PVDF [28-29]. On the contrary, epoxy:PTh samples (5 wt. % PTh nanoparticles) showed an electrical conductivity of 10^{-5} S/cm [27]. Therefore, electrical dc conductivity results reveal a significant improvement in dc conductivity for semiconducting SEP/P3TMA films with high P3TMA wt. % content when tested at high temperatures.

Electrochemical impedance spectroscopy (EIS) analyses were carried out to obtain bulk resistance and interfacial properties of CPnC films containing 0, 1 and 5 wt. % P3TMA (cured at RT and T60), since those were the compositions that exhibited better mechanical properties and/or whose electrical dc conductivity values were not measured by the two-point probe procedure. This electrochemical technique is a powerful tool to estimate the through-plane conductivity of polymeric films after accurate fitting of the impedance data to an equivalent electrical circuit (EEC). If the cell architecture and

contact electrodes are well-mounted, both insulating and conducting samples can be tested using EIS [36-38].

Samples were prepared following the same procedure: appropriated films of 1.5 cm diameter were cut and sandwiched between two stainless steel electrodes, separated by a Teflon holder, corresponding to a through-plane conductivity homemade cell configuration, which was fully described in a previous work [39]. Samples were immersed in a PBS solution for 24h prior the measurement, and the excess of surface water was removed with blotting paper before each assay. In our system, ions (from the electrolyte solution), the counter-ion (Cl^-) and holes (present along the doped P3TMA polymeric chains) act as charge carriers and establish electron transport paths through the volume of the sample when an AC potential is applied.

Figure 5 shows the Nyquist and Bode plots obtained for films containing 1 wt. % P3TMA, cured at RT and T60. The Nyquist spectra show a first semicircle in the high frequency range, a second semicircle in the low frequency range, and finally an inclined straight line at a constant angle. Firstly, the electrical behavior of SEP/P3TMA-R1films cured at RT and 60 ºC is very similar, and only differs in the diameter of the second semi-circle, which is smaller for the former than for the latter. This difference is also appreciated in the Bode plot, where the overall impedance is slightly higher for the film cured at 60 ºC. Moreover, phase angles for both samples are found around 40-50º and 20º at high and low frequencies, respectively, independently of the curing temperature. For samples containing 5 wt. % P3TMA, two semi-circles are also detected (Figure 6a) although they are much smaller compared to those displayed by SEP/P3TMA-R1 samples. Moreover, SEP/P3TMA-R5 cured at high temperature (T60) exhibit bigger semi-circles, thus indicating higher resistance values than SEP/P3TMA-R5 films cured at RT. In this case, phase angles for SEP/P3TMA-R5 (RT) / SEP/P3TMA-R5 (T60)

samples are detected around 27º/ 53º and 30º / 35º at high and low frequencies, respectively (Figure 6b).

EIS experimental data was satisfactorily fitted with the EEC depicted in Figure 7a, which is $(R_1CPE_1)(CPE_2[R_2CPE_3])$. The fitting quality was judged based on the error percentage associated to each circuit component, showing errors lower than 10%. Ideal capacitor elements were replaced by constant phase elements (CPE), which describe non-ideal capacitor when the phase angle is different from -90º. The CPE impedance is attributed to the distributed surface reactivity, surface heterogeneity, and roughness, non-uniform current and potential distribution, which in turn are related to the electrode geometry and the electrode porosity [40]. The high-frequency semicircle observed, which is described by the parallel combination of R_1 and CPE_1, is ascribed to the combination of the bulk resistance and the effects of dielectric relaxations of the polymeric system [36]. Nevertheless, impedance behavior described by Nyquist plots showing more than one semicircle or Bode plots exhibiting different capacitive/resistive regions may describe systems with several phases, which is our case. Thus, the second resistor/capacitor parallel combination (R_2 and CPE_2) also corresponds to the film bulk properties. Both semicircles account for conductive pathways created across the polymer film. Finally, PBS absorption and penetration into small defects present in the films, such as small pores, would eventually create new electrode-electrolyte interfaces, which appear as the straight line inclined at a constant angle at low frequencies, and is described as a double-layer capacitance (CPE_3).

SEP/P3TMA-R0 samples (cured at RT and at 60 ºC) were also tested. The membrane resistance for these insulating samples is extremely high (inset of Figure 6a), thus the resulting EIS spectra is not a semi-circle but a straight line slightly bended, which corresponds to the membrane resistance modelled in parallel with a capacitor element

(EEC showed in Figure 7b). SEP/P3TMA-R1 films display similar bulk resistance values regardless the curing temperature (Table 3). The low P3TMA content results in the same degree of particle dispersion and aggregation, thus both samples present similar potential charge carriers density. Accordingly, SEP/P3TMA-R5 cured at RT shows reduced resistance values (R_1 and R_2) because of the higher P3TMA content, whereas for SEP/P3TMA-R5 (T60) both R_1 and R_2 are the higher resistance values. In this particular case, the mobility of the network is the dominant factor. The rigid polymer backbone of SEP/P3TMA-R5 (T60) leads to a low density of potential charge carriers, thus influencing the bulk resistance. Finally, the conductivity values for CPnC films (Table 3) were calculated by the following equation considering each film thickness:

$$\delta = \frac{1}{R}\frac{d}{S} \qquad (2)$$

where δ is the bulk conductivity (S/cm), d is the film thickness, S is the area of electrodes contacting the polymeric film (1.767 cm^2) and R (Ω) is the bulk film resistance (R_1 or R_2).

The addition of P3TMA particles to the epoxy matrix results in an enhancement of films conductivity with respect to the pure epoxy films (SEP/P3TMA-R0). Furthermore, EIS results indicate that both the filler concentration and the mobility of the polymeric matrix play an important role on the electrical properties displayed by CPnC samples.

SEM and AFM observations

Finally, this section evaluates the distribution of P3TMA particles into the epoxy matrix using cross-sectional films containing different P3TMA.

Figure 8 shows representative SEM micrographs of films containing 0, 1, 12 and 25 wt.% P3TMA cured at RT (left column) and T60 (right column). Both epoxy films,

cured at RT and T60, (Figure 8a) exhibit a perfectly smooth surface only disrupted by marks arising from the fracture procedure. In contrast, CPnC films with only 1 wt.% P3TMA show surface irregularities, independently of the curing temperature (Figure 8b). This effect is more pronounced in CPnC films containing high content of P3TMA, as expected. For example, in SEP/P3TMA-R5 (RT) CP nanoparticles of around 80-100 nm were detected. These nanoparticles tend to form aggregates of ~ 250 nm in films cured at T60 and of near 0.45-1.6 μm when the curing process takes place at RT. SEM micrographs from SEP/P3TMA-R12 and SEP/P3TMA-R25 films (Figure 8c-d) reveal the evolution of such P3TMA aggregation. SEP/P3TMA-R12 (T60) films are rougher than SEP/P3TMA-R1 (T60) CPnC films (Figure 8b). Finally, both SEP/P3TMA-R25 cured at RT and T60 films (Figure 8d) are characterized by a much rougher cross-section surface than the previous CPnC samples.

Roughness values were checked with AFM technique. Results indicate that high concentrations of P3TMA nanoparticles provoke high surface roughness on CPnC films, as previously observed by SEM. RMS Rq values increases nearly two-fold, from 14.1 ± 2.7 nm to 27.0 ± 9.0 nm, when the concentration of P3TMA grows from 1 to 25 wt. % for films cured at room temperature, compared to films cured at 60ºC. On the other hand, for films cured at T60, the RMS Rq increases 4.5 nm with P3TMA concentration (*i.e.* from 1.2 ± 0.1 nm to 5.7 ± 1.1 nm). Therefore, RMS Rq values are significantly lower for films cured at 60ºC than at RT, corroborating with a better dispersed P3TMA particles at high temperature.

In conclusion, P3TMA particles are entrapped in the epoxy matrix when fast cross-liking takes place at high curing temperatures, which induces phase separation. Oppositely, slow curing forms larger aggregates as P3TMA nanoparticles are attracted by electrostatic interactions. Thus, P3TMA-solvent compatibility and the curing

temperature are the two main parameters that have to be controlled to avoid P3TMA agglomeration.

Conclusions

CPnCs have been successfully prepared by loading an epoxy resin with P3TMA nanoparticles dispersed in THF, thus overcoming effectively the typical limitations of CPs such as reduced solubility and difficult processability. By preventing the incompatibility between the CP and the solvent, excessive nanoparticle aggregation was avoided during CPnC films processing. However, the final dispersion and size agglomeration of P3TMA particles is mainly affected by the curing temperature. Results from both UV-vis spectra and SEM observations allow us to conclude that fast cross-linking induces phase separation at the microscopic scale. P3TMA nanoparticles are entrapped quicker in the epoxy matrix when curing occurs at 60 ºC, whereas slow curing leads to larger aggregates formed by electrostatic forces attracting P3TMA moieties.

These two scenarios are found to affect considerably the mechanical and electrical properties of CPnC films. Firstly, the addition of P3TMA nanoparticles increases the Young's modulus values for CPnC films independently of the curing temperature. Similarly, tensile strength values are also influenced by both the curing temperature and the P3TMA wt. % content, while the strain at break response of SEP/P3TMA-RX films remains unaltered. Secondly, regarding to the electrical properties, results are satisfactory for nanocomposites with the highest P3TMA wt. % content. Bulk conductivities determined by the two-point probe method are $6.0 \cdot 10^{-7}$ - $7.2 \cdot 10^{-7}$ S/cm and $6.5 \cdot 10^{-7}$ - $8.2 \cdot 10^{-7}$ S/cm for SEP/P3TMA-R12 and SEP/P3TMA-R25 samples, respectively. Epoxy-rich regions prevent P3TMA particles to be efficiently

interconnected within the insulating polymeric matrix, thus hindering the creation of conductive paths and reducing the sample conductivity. Nevertheless, CPnC films exhibit a semiconductor behavior and measurements indicate a significant increase in conductivity values when compared to that of the pure epoxy. Finally, EIS observations confirm that the addition of P3TMA particles leads to a reduction in the resistance of CPnC films, which is affected by the network mobility and the charge carrier density.

Using this procedure, we were able to obtain SEP/P3TMA-RX films with tailored features (good mechanical response and enhanced electrical properties) for advanced technological applications. Overall, the suitable combination of properties in hybrid materials is a challenging task, which relies on fulfilling rigorous requirements: (1) excellent compatibility between the matrix and the filler, thus resulting in satisfactory features, (2) feasible procedure and scalability, and (3) optimized procedure costs.

Acknowledgements

Financial support from the MICINN and FEDER (MAT2012-34498) and Generalitat de Catalunya (research group 2009 SGR 925 and XRQTC) is gratefully acknowledged. Support for the research of C.A. was received through the prize "ICREA Academia" for excellence in research funded by the Generalitat de Catalunya. M. M. P.-M. thanks the financial support through a FPI-UPC grant. We also thank Dr. Carlos Díaz Blanco from GBMI (Molecular and Industrial Biotechnology Group, UPC) for technical support during SLS measurements.

References

1. S. S. Mahapatra, S. K. Yadav, and J.W. Cho, *React. Funct. Polym.*, **72**, 227 (2012).

2. S. S. Mahapatra and N. Karak, *Mater. Chem. Phys.*, **112**, 1114 (2008).

3. H. A. Al-Turaif, *Prog. Org. Coat.*, **69**, 241 (2010).

4. Y. Li, Y. Iwakura, L. Zhao, and H. Shimizu, *Macromolecules*, **41**, 3120 (2008).

5. F. Carpi and D. De Rossi, *IEEE T. Inf. Technol. B*, **9**, 295 (2005).

6. Y. Ding, M. A. Invernale, and G. A. Sotzing, *ACS Appl. Mater. Interfaces*, **2**, 1588 (2010).

7. M. Park, J. Cheng, J. Choi, J. Kim, and J. Hyun, *Colloids Surf. B*, **102**, 238 (2013).

8. R. Perumalraj, A. Anilkumar, A. S. Nirmala Devi, B. Saranya, P. Deepa, R. Karthika, and N. Maheshwari, *J. Reinf. Plast. Compos.*, **30**, 203 (2010).

9. T. Sekitani, Y. Noguchi, K. Hata, T. Fukushima, T. Aida, and T. Someya, *Science*, **321**, 1468 (2008).

10. M. Donolato, C. Tollan, J. M. Porro, A. Berger, and P. Vavassori, *Adv. Mater.*, **25**, 623 (2013).

11. K.-Y. Chun, Y. Oh, J. Rho, J.-H. Ahn, Y.-J. Kim, H. R. Choi, and S. Baik, *Nat. Nanotech.*, **5**, 853 (2010).

12. M. G. Urdaneta, R. Delille, and E. Smela, *Adv. Mater.*, **19**, 2629 **(2007).**

13. H. Stoyanov, M. Kollosche, S. Risse, D. N. McCarthy, and G. Kofod, *Soft Matter*, **7**, 194 (2011)**.**

14. R. Pelrine, R. Kornbluh, Q. Pei, and J. Joseph, *Science*, **287**, 836 (2000).

15. G. Gallone, F. Galantini, and F. Carpi, *Polym. Int.*, **59**, 400 (2010).

16. E. Miyako, C. Hosokawa, M. Kojima, M. Yudasaka, R. Funahashi, I. Oishi, Y. Hagihara, M. Shichiri, M. Takashima, K. Nishio, and Y. Yoshida, *Angew. Chem. Int. Ed.*, **50**, 12266 (2011).

17. A. Mandal and A. K. Nandi, *J. Phys. Chem. C*, **116**, 9360 (2012).

18. B. S. Shim, W. Chen, C. Doty, C. Xu, and N. A. Kotov, *Nano Lett.*, **8**, 4151 (2008).

19. N. G. Sahoo, S. Rana, J. W. Cho, L. Li, and S. H. Chan, *Prog. Polym. Sci.*, **35**, 837 **(2010).**

20. T.-L. Wang, C.-H. Yang, Y.-T. Shieh, and A.-C. Yeh, *Eur. Polym. J.*, **45**, 387 (2009).

21. M. Tiitu, A. Talo, O. Forsén, and O. Ikkala, *Polymer*, **46**, 6855 (2005).

22. M. E. Leyva, F. G. Garcia, A. A. A de Queiroz, and D. A. W. Soares, *J. Mater. Sci.: Mater. Electron.*, **22**, 376 **(2011).**

23. S. Desvergne, A. Gasse, and A. Pron, *J. Appl. Polym. Sci.***, 120,** 1965 (2011).

24. F. Carpi, G. Gallone, F. Galantini, and D. De Rossi, *Adv. Funct. Mater.*, **18**, 135 (2008).

25. A. Mandal, and A. K. Nandi, *Macromol. Chem. Phys*., **212**, 1636 (2011).

26. A. J. Granero, P. Wagner, K. Wagner, J. M. Razal, G. G. Wallace, and M. in het Panhuis, *Adv. Funct. Mater.*, **21**, 955 (2011).

27. O. Zabihi, A. Khodabandeh, and S. M. Mostafavi, *Polym. Degrad. Stab.*, **97**, 3 (2012).

28. S. Manna, A. Mandal, and A. K. Nandi, *J. Phys. Chem. B*, **114**, 2342 (2010).

29. A. L. Gomes, M. B. Pinto Zakia, J. G. Filho, E. Armelin, C. Alemán, and J. Sinezio de Carvalho Campos, *Polym. Chem.*, **3**, 1334 (2012).

30. B. Kim, L. Chen, J. Gong, and Y. Osada, *Macromolecules*, **32**, 3964 (1999).

31. J. M. de Souza, and E. C. Pereira, *Synth. Met.*, **118**, 167 (2001).

32. A. L. Gomes, J. Casanovas, O. Bertran, J. S. d. C. Campos, E. Armelin, and C. Alemán, *J. Polym. Res.*, **18**, 1509 (2011).

33. G. Zotti, S. Zecchin, G. Schiavon, and B. Vercelli, *Chem. Mater.*, **15**, 2222 (2003).

34. F. Zhang, and M. P. Srinivasan, *Thin Solid Films*, **479**, 95 (2005).

35. F. Zhang, and M. P. Srinivasan, *Mater. Chem. Phys.*, **112**, 223 (2008).

36. I. R. Rodrigues, M. M. de Camargo Forte, D. S. Azambuja, and K. R. L. Castagno, *React. Funct. Polym.*, **67**, 708 (2007).

37. M. A. Milani, D. González, R. Quijada, N. R. S. Basso, M. L. Cerrada, D. S. Azambuja, and G. B. Galland, *Compos. Sci. Technol.*, **84**, 1 (2013).

38. F. C. Fim, N. R. S. Basso, A. P. Graebin, D. S. Azambuja, and G.B. Galland, *J. Appl. Polym. Sci.*, **128**, 2630 (2013).

39. F. Müller, C. A. Ferreira, D. S. Azambuja, C. Alemán, and E. Armelin, *J. Phys. Chem. B*, **118**, 1102 (2014).

40. J.-B. Jorcin, M. E. Orazem, N. Pébère, and B. Tribollet, *Electrochim. Acta*, **51**, 1473 (2006).

Table 1. Values of λ_{max}, λ_{onset} and E_g obtained from the UV-vis absorption spectra of CPnC films cured at 60 ºC. Data from the spectrum of a dilute P3TMA solution (0.001 wt. %) in THF are also displayed for comparison.

Conditions	λ_{max} **(nm)**	λ_{onset} **(nm)**	E_g **(eV)**
P3TMA (0.001 wt. %)	383	475	2.62
SEP/P3TMA-R1	400	520	2.39
SEP/P3TMA-R3	404	527	2.36
SEP/P3TMA-R5	482	552	2.25
SEP/P3TMA-R12	505	582	2.13
SEP/P3TMA-R25	538	627	1.98

Table 2. Summary of the mechanical properties for the epoxy and CPnC films cured at at 60 ºC.

Sample	Young's Modulus (MPa)	Strain at break (%)	Tensile Strength (MPa)
SEP/P3TMA-R0	825 ± 142	5.2 ± 1.1	42 ± 7
SEP/P3TMA-R1	1010 ± 204	5.0 ± 0.5	54 ± 4
SEP/P3TMA-R3	1071 ± 167	5.5 ± 0.3	54 ± 4
SEP/P3TMA-R5	1192 ± 164	5.9 ±0.4	63 ± 4
SEP/P3TMA-R12	1179 ± 171	6.6 ± 0.7	56 ± 4
SEP/P3TMA-R25	831 ± 164	1.1 ± 0.3	12 ± 4

Table 3. Bulk resistance and conductivity data calculated by EIS for samples containing 1 and 5 wt.% P3TMA and pure epoxy films.

Sample	R_1 ($Ohm \cdot cm^2$)	σ_1 (S/cm)	R_2 ($Ohm \cdot cm^2$)	σ_2 (S/cm)
SEP/P3TMA-R0	$1.1 \cdot 10^{8}$	$1.4 \cdot 10^{-10}$	-	-
SEP/P3TMA-R1 (RT)	$9.4 \cdot 10^{4}$	$1.4 \cdot 10^{-7}$	$2.9 \cdot 10^{5}$	$4.6 \cdot 10^{-8}$
SEP/P3TMA-R1 (T60)	$7.8 \cdot 10^{4}$	$1.5 \cdot 10^{-7}$	$5.1 \cdot 10^{5}$	$2.3 \cdot 10^{-8}$
SEP/P3TMA-R5 (RT)	$5.1 \cdot 10^{4}$	$1.2 \cdot 10^{-7}$	$6.2 \cdot 10^{4}$	$9.7 \cdot 10^{-8}$
SEP/P3TMA-R5 (T60)	$1.1 \cdot 10^{5}$	$5.0 \cdot 10^{-8}$	$6.9 \cdot 10^{5}$	$8.1 \cdot 10^{-9}$

Captions to Figures

Figure 1. FTIR spectra of P3TMA (dashed line) nanoparticles, SEP/P3TMA-R0 (dotted line), SEP/P3TMA-R1 (black continuous line) and SEP/P3TMA-R25 (grey continuous line) samples cured at 60 ºC. Labels A, B, C and C' absorption bands are described in Results and Discussion section.

Figure 2. UV-vis absorption spectra for CPnC films cured at 60 ºC. Dotted line corresponds to the diluted P3TMA in THF solution, dashed lines correspond to the spectra of the epoxy resin without P3TMA (SEP/P3TMA-R0), whereas continuous lines are related to different compositions of CPnC (SEP/P3TMA-RX) transparent films.

Figure 3. Schematic representation of SEP/P3TMA CPnC preparation employing room temperature (RT) and thermally activated curing processes (T60). SEM micrographs are illustrative of good dispersion (small particle aggregation at T60) and bad dispersion (large particle aggregation at RT) when content of P3TMA nanoparticles have increased.

Figure 4. (a) Stress-strain curves for CPnC films cured at 60 ºC and (b) Young's modulus for CPnC films as a function of the P3TMA wt. % content and cure temperature (RT and T60).

Figure 5. (a) Nyquist and (b) Bode plots for SEP/P3TMA-R1 films at RT (□, ■) and T60 (○, ●). Symbols correspond to experimental data, while lines are fitted curves.

Figure 6. (a) Nyquist and (b) Bode plots for SEP/P3TMA-R5 films at RT (□, ■) and T60 (○, ●). Symbols correspond to experimental data, while lines are fitted curves. Insets correspond to SEP/P3TMA-R0 electrical response.

Figure 7. Equivalent electric circuit used for fitting EIS data from CPnC samples (a) and pure epoxy (b).

Figure 8. Typical cross-sectional SEM micrographs (SE2 detector) for the epoxy and CPnC films cured at room temperature (left column) and at 60ºC (right column): (a) SEP/P3TMA-R0, (b) SEP/P3TMA-R1, (c) SEP/P3TMA-R12 and (d) SEP/P3TMA-R25 samples (* indicates epoxy-rich regions).

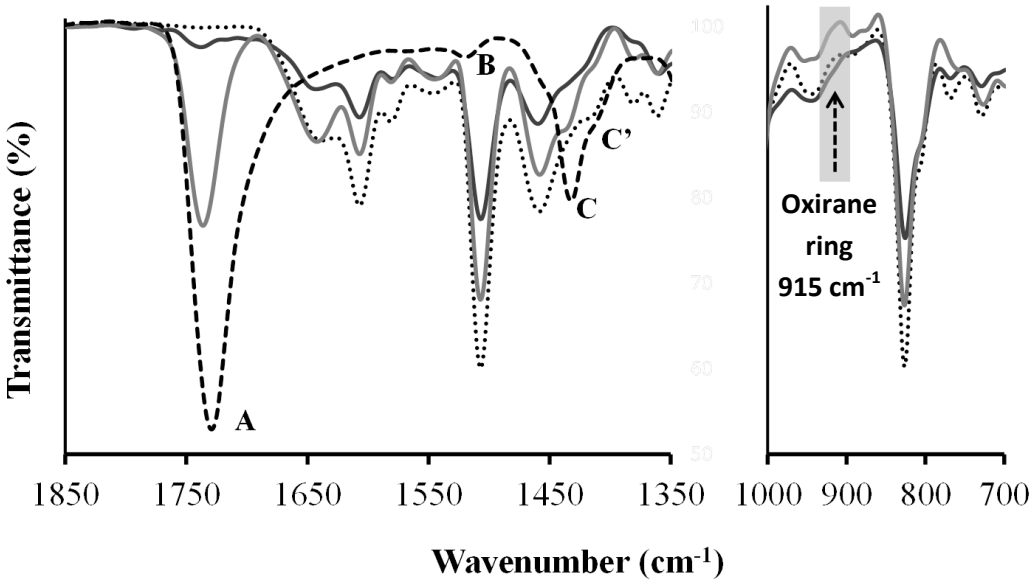
Transmittance (%)
A
B
C
C'
Oxirane
ring
915 cm-1
1850
1750
1650
1550
1450
1350
1000
900
800
700
Wavenumber (cm-1)

Figure 1

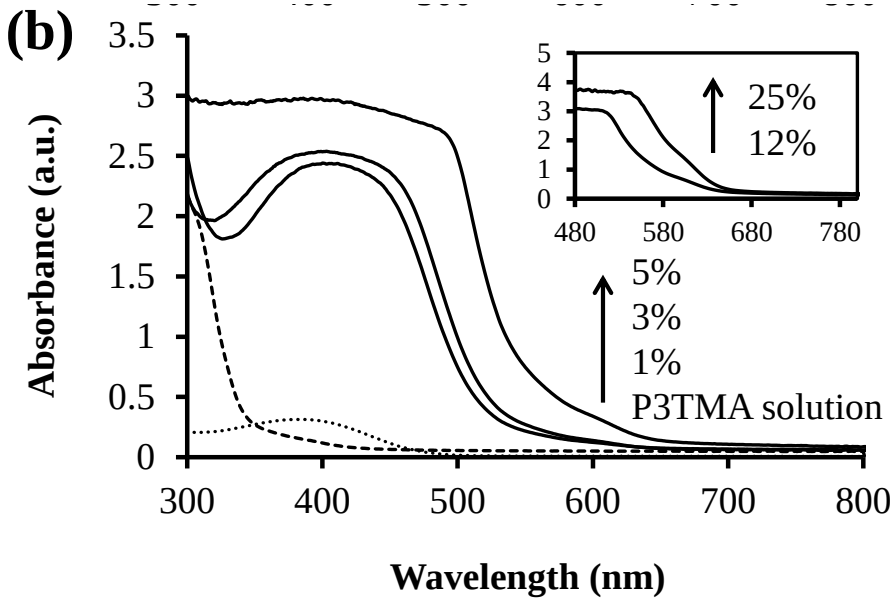
(b)
Absorbance (a.u.)
3.5
3
2.5
2
1.5
1
0.5
0
300
400
500
600
700
800
Wavelength (nm)
5
4
3
2
1
0
480
580
680
780
25%
12%
5%
3%
1%
P3TMA solution

Figure 2

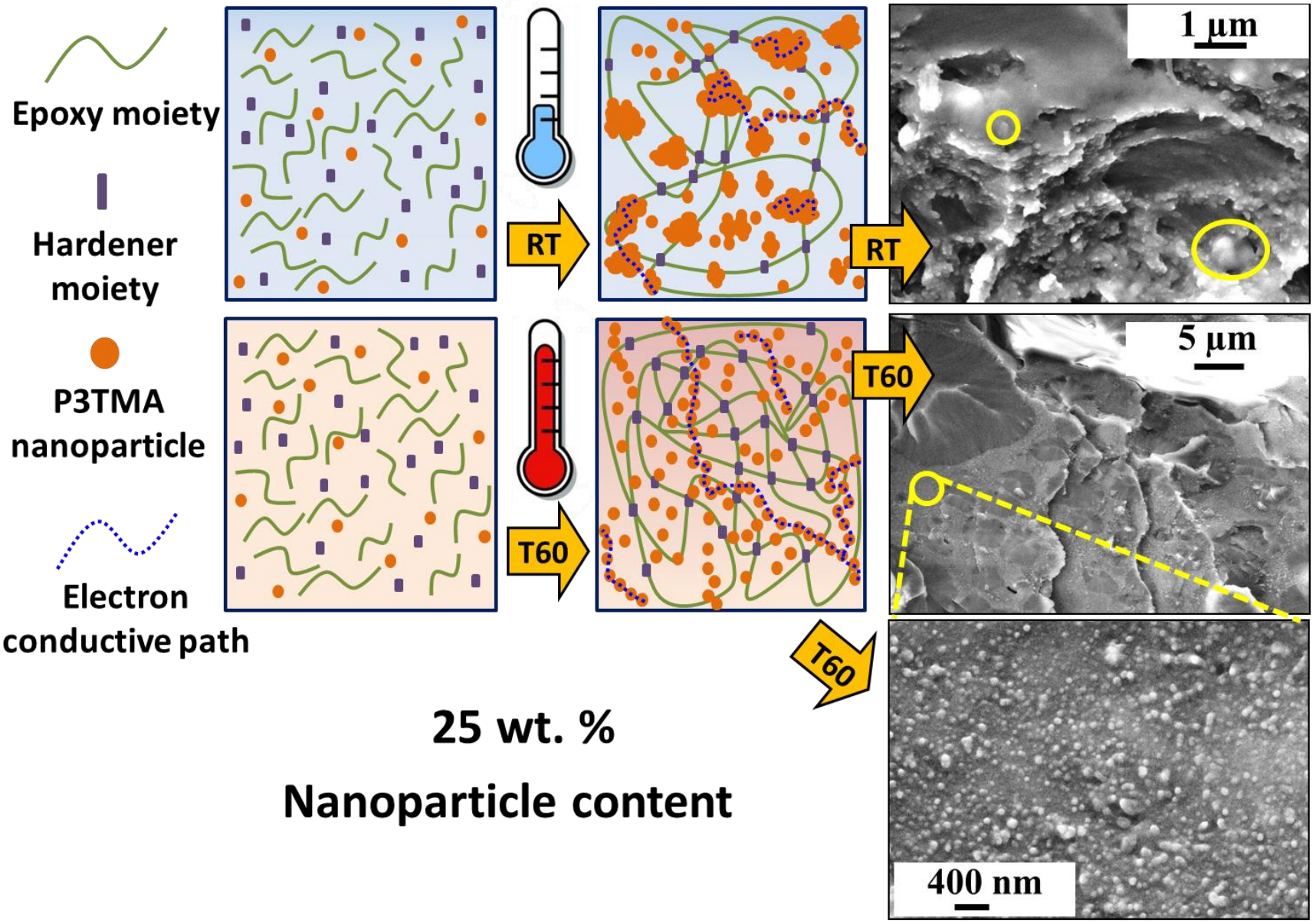
Epoxy moiety
Hardener moiety
P3TMA nanoparticle
Electron conductive path
RT
RT
T60
T60
T60
1 µm
5 µm
400 nm
25 wt. %
Nanoparticle content

Figure 3

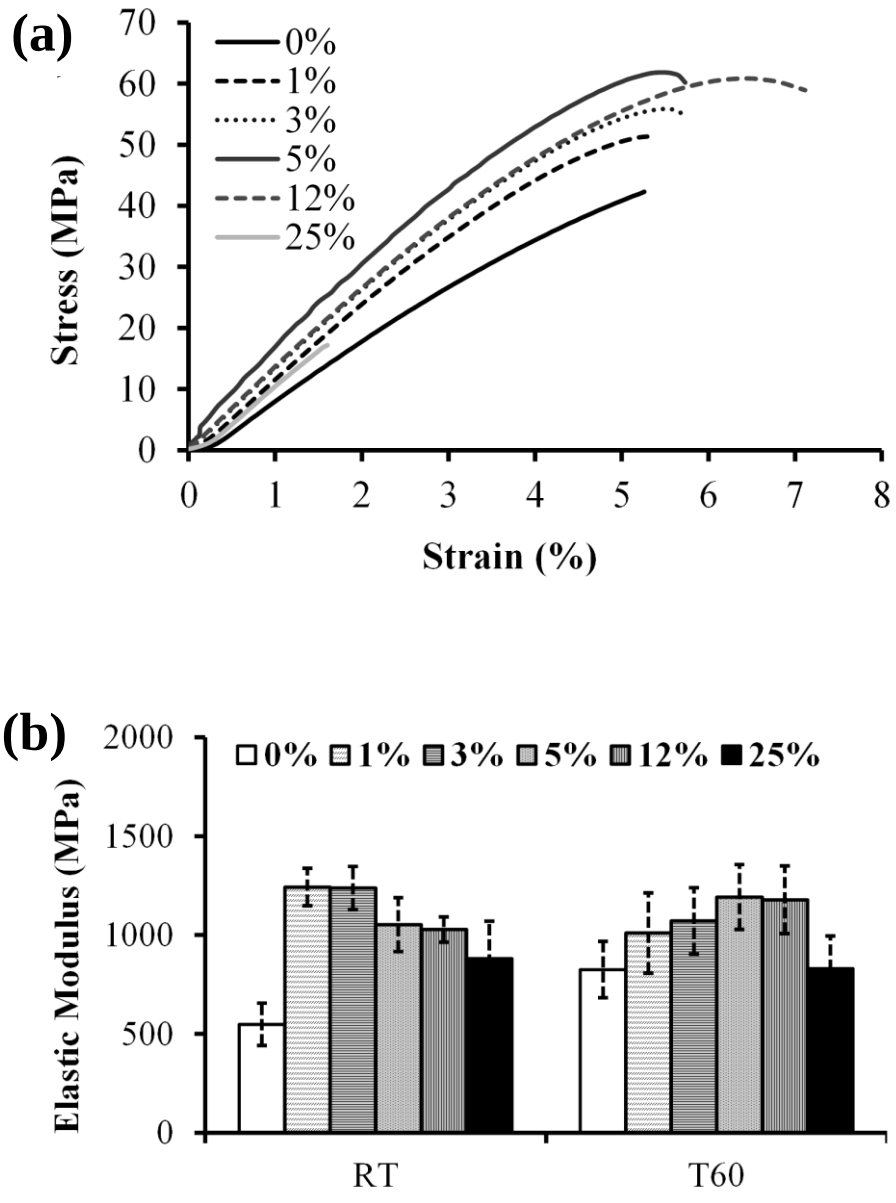
(a)
Stress (MPa)
Strain (%)
0%
1%
3%
5%
12%
25%
0
10
20
30
40
50
60
70
0
1
2
3
4
5
6
7
8
(b)
Elastic Modulus (MPa)
0% 1% 3% 5% 12% 25%
0
500
1000
1500
2000
RT
T60

Figure 4

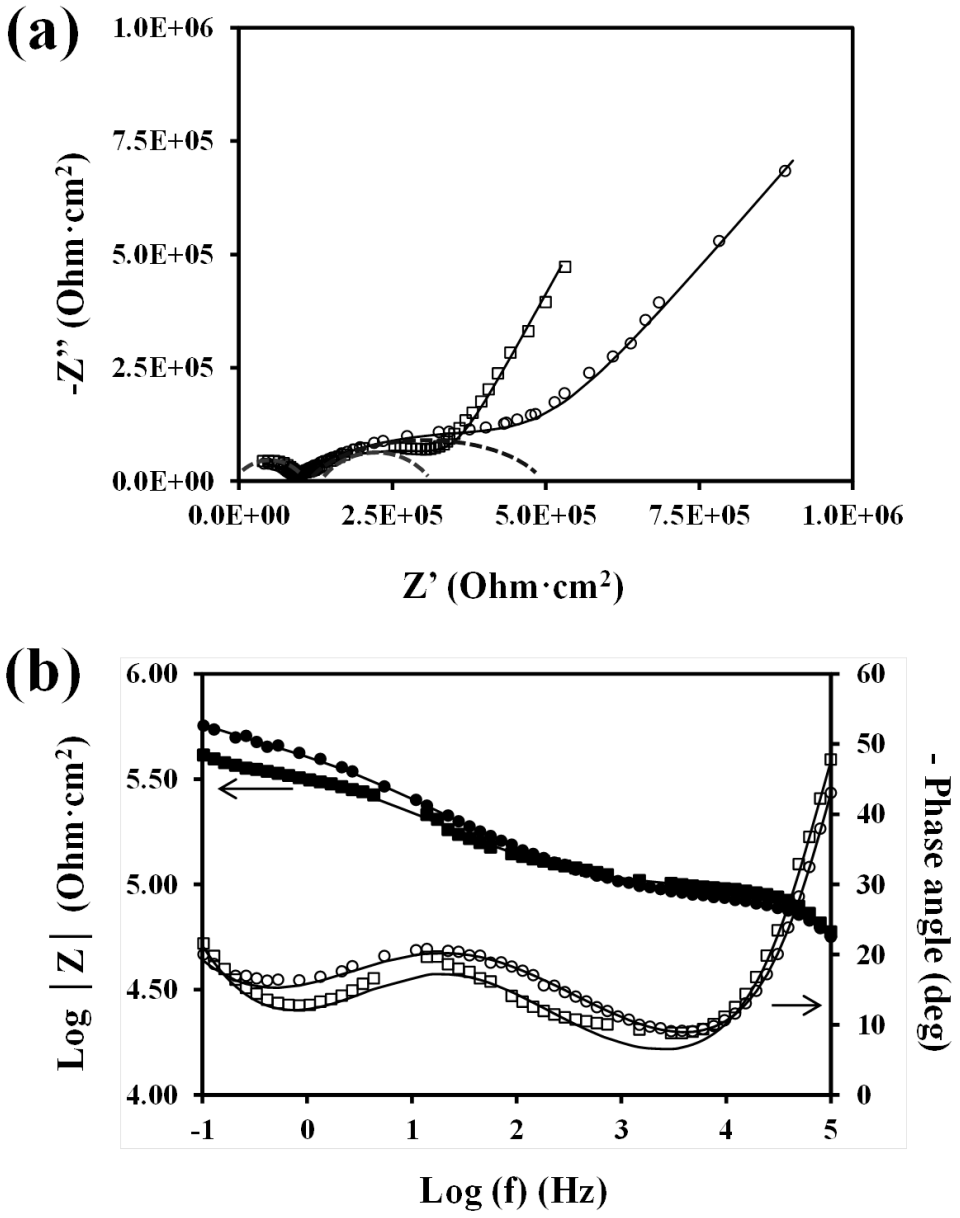
(a)
1.0E+06
7.5E+05
5.0E+05
2.5E+05
0.0E+00
-Z'' (Ohm·cm²)
0.0E+00
2.5E+05
5.0E+05
7.5E+05
1.0E+06
Z' (Ohm·cm²)
(b)
6.00
5.50
5.00
4.50
4.00
Log |Z| (Ohm·cm²)
60
50
40
30
20
10
0
- Phase angle (deg)
-1
0
1
2
3
4
5
Log (f) (Hz)

Figure 5

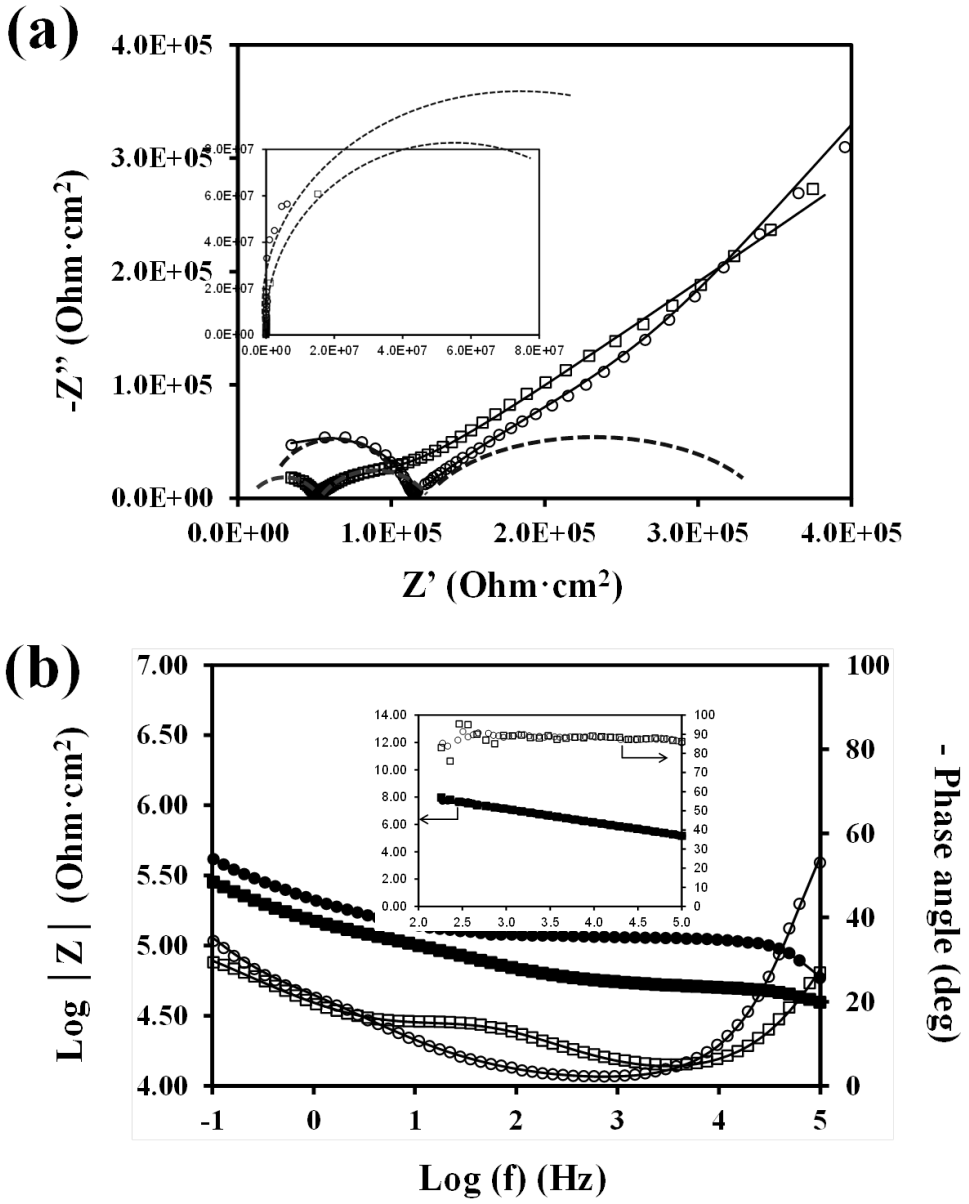
(a)
4.0E+05
3.0E+05
2.0E+05
1.0E+05
0.0E+00
-Z'' (Ohm·cm²)
0.0E+00
1.0E+05
2.0E+05
3.0E+05
4.0E+05
Z' (Ohm·cm²)
8.0E+07
6.0E+07
4.0E+07
2.0E+07
0.0E+00
0.0E+00
2.0E+07
4.0E+07
6.0E+07
8.0E+07
(b)
7.00
6.50
6.00
5.50
5.00
4.50
4.00
Log |Z| (Ohm·cm²)
-1
0
1
2
3
4
5
Log (f) (Hz)
100
80
60
40
20
0
- Phase angle (deg)
14.00
12.00
10.00
8.00
6.00
4.00
2.00
0.00
2.0
2.5
3.0
3.5
4.0
4.5
5.0
100
90
80
70
60
50
40
30
20
10
0

Figure 6

(a)

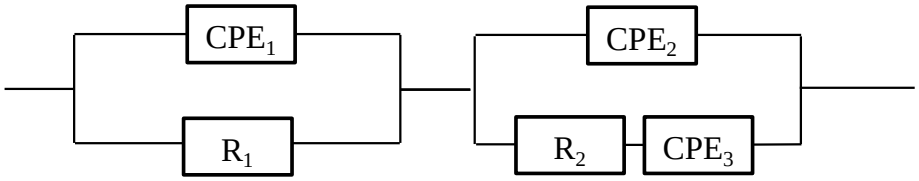

(b)

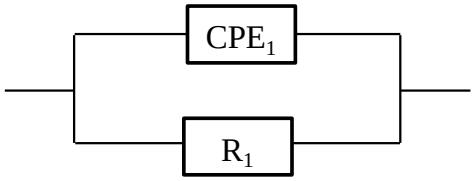

Figure 7

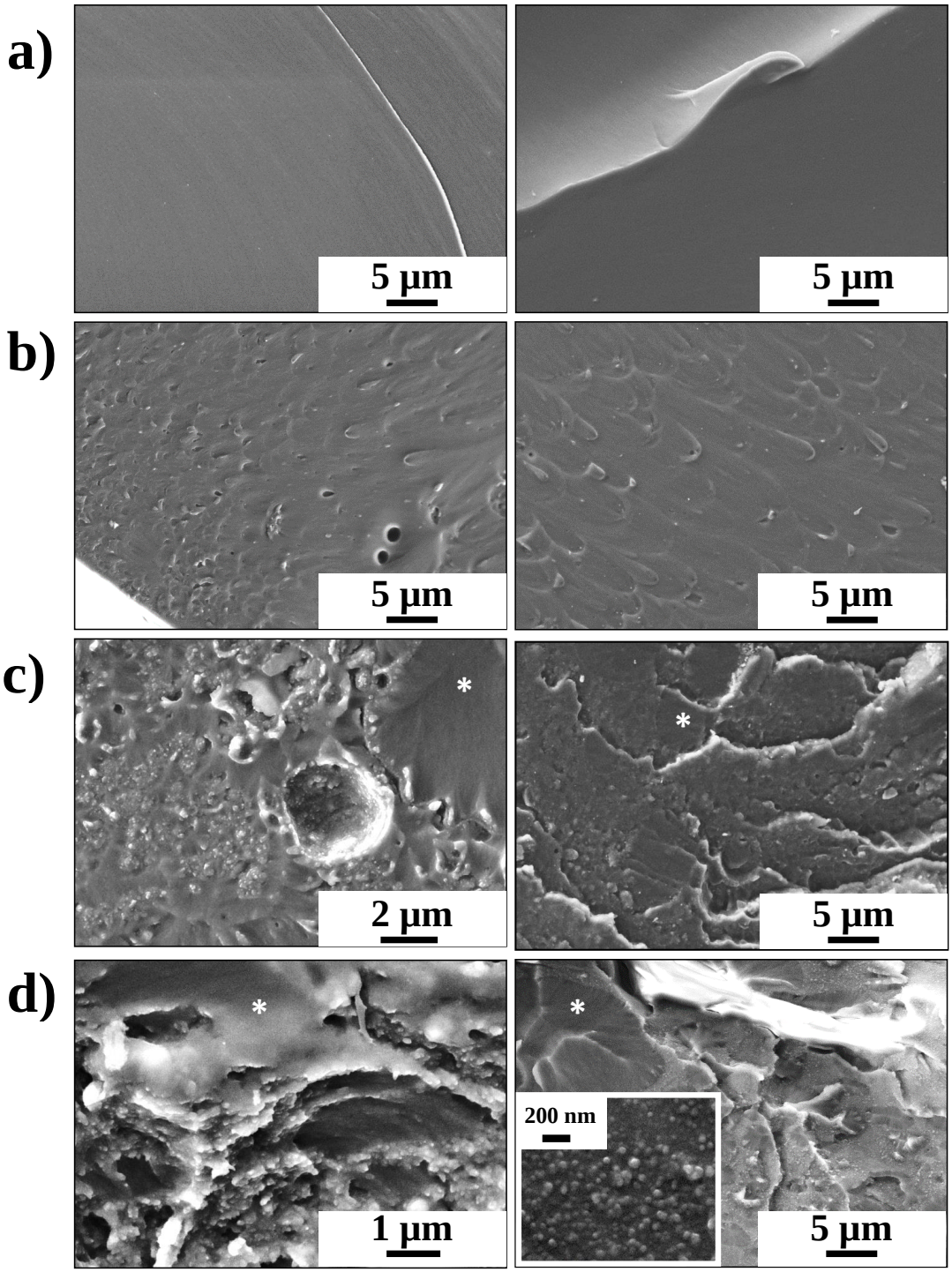

Figure 8